TWMS J. App. Eng. Math. V.8, N.1a, 2018, pp. 193-207

MODELING OF COMBINED NATURAL/THERMOCAPILLARY CONVECTION FLOWS IN GERMANIUM MELT AT HIGH TEMPERATURES

F. MECHIGHEL[1], N. ARMOUR[2], S. DOST[2], §

Abstract. A mathematical model for the description of combined natural/ thermocapillary convection melt flows in cylindrical (3D) geometry is developed. It is utilized to model germanium melt convective flows in an *isothermal* experimental crucible setup. This experimental setup is devised exclusively to study the dissolution phenomenon of silicon into germanium melt. In this system, the germanium melt is subjected to higher temperatures. Using a simplified axisymmetric (2D) model, numerical simulations are carried out to examine the combined natural/thermocapillary flows developing in the germanium melt. Pure thermocapillary and pure natural convective flows are also studied numerically.

Keywords: Germanium melt, free surface, Marangoni convection, natural (thermal or buoyant) convection, mathematical modeling, numerical simulation.

AMS Subject Classification: 76M10

1. Introduction

Silicon germanium (SiGe) is a promising single crystal material which is very valuable in the electronics and optoelectronics industry mainly in the Heterojunction Bipolar Transistor HBT technology [1, 2]. In order to produce such crystals several crystal growth techniques are used [3]. For instance the Czochralski (Cz) [4], Floating zone (Fz) [5], horizontal boat Bridgman (HB) [6], liquid encapsulated zone melting [7] and the liquid phase diffusion (LPD) (also recognized as the multicomponent zone melting (MCZM) [8]).

Among these the most important crystal growth techniques containing free surfaces are the Fz technique and the Cz method. In these techniques, generally, a melting zone (liquid phase) is slowly solidified as a cylindrical crystal, vertically oriented. For instance in Fz, the liquid phase between the feed and seed crystals is held by the *surface tension*. A free surface tension is also present in Cz. Thus, when a free surface exists in a crystal growth technique, the thermocapillary (or Marangoni) convection flow develops in the melt, driven by surface tension, and plays an important role in producing homogeneous crystals with uniform properties [9, 10].

[1] LR3MI Laboratory, Mechanical Engineering Department, Science of Engineering Faculty, PB 12. University of Annaba, Annaba 23000, Algeria.
e-mail: farid.mechighel@univ-annaba.dz; ORCID: https://orcid.org/0000-0002-4726-7613.

[2] Crystal Growth Laboratory, University of Victoria, Victoria, BC, Canada, V8W 3P6.
ORCID: https://orcid.org/0000-0003-2714-8905.
e-mail: sdost@me.uvic.ca; ORCID: https://orcid.org/ 0000-0002-6310-6043.

§ Manuscript received: April 12, 2018; accepted: June 09, 2018.

Marangoni convection is also present in the experimental setup considered and investigated in the present work [11, 12]. The setup consists of a crucible similar to that used in the Melt-Replenishment Czochralski and LPD growth systems (schematically shown in Fig. 1). This experimental setup was exclusively devised to examine the effects of free surface. Indeed, in order to investigate the effect of free surface on silicon *dissolution* in germanium melt two sets of experiments, with a free surface and without a free surface were developed [12].

Experiments showed that the convective flows developing in the melt play a key role in the dissolution behavior. In particular, it was shown that the Marangoni convection had an important effect on the *mixing* and on the *shape* of dissolution interface [12]. The experimental results indicate that silicon dissolution from the bottom of the melt in the presence of a free surface will occur faster and be subject to *instability* and melt inhomogeneity. Accordingly, an appropriate numerical study for the combined surface tension and buoyancy driven convection flows in the germanium melt is important for a better understanding of the behavior and structure of melt flows in the system. The knowledge of the behavior of germanium melt flows at high temperatures is also essential in the growth of SiGe single crystals by other growth techniques [12].

In the present paper the problem of combined natural/thermocapillary convection in a cylindrical (three-dimensional 3D) geometry with free surface is modeled mathematically. The emphasis is on the isothermal experimental crucible setup shown in Fig. 1. Indeed, the model is adapted to model this system. The combined natural/ thermocapillary convection flows in the Ge melt was investigated by numerical simulations using an axisymmetric (two-dimensional 2D) model, and in order to provide further insight into the nature of these melt flows, in the present crucible setup, numerical simulations were also carried out for thermocapillary convection flows and natural convection independently.

2. General considerations and mathematical model

2.1. **Governing equations for the physical problem.** Consider the Ge melt system in the experimental configuration shown in Fig. 1. The melt, initially at the temperature $T_{ini} = 1073K$, is maintained in the quartz crucible/ampoule system as shown in Fig.1. In this system, the ampoule bottom of radius, $(r = R = d/2 = 11mm)$, located at $z = 0$, bounds the melt from below in the horizontal plane. The melt is bounded from the sides (in azimuthal-direction) by the ampoule wall. The horizontal upper boundary is the free surface of *mean* surface tension,σ_0, and is located at $(z = h = 25mm)$. All the walls of the crucible/ampoule system are assumed *rigid* and *stationary*. By referring to Fig.1, the free surface is defined as the interface melt/vacuum separating the melt from the vacuum. In the present study, the vacuum is assumed as a gas with very small viscosity and thermal diffusivity. Under these conditions the height of the melt is $h = 25mm$ and thus its volume is $V_{melt} \approx 9503mm^3$. While, the surface of the free surface is $S_{int} = \pi d^2/4 \approx 380mm^2$.

In the experiment, the crucible/ampoule walls are maintained at the *constant* temperature of $T_h \equiv T_B = 1373K$ and the heat flux on the upper free surface (interface melt/vacuum) is set to be zero, $\dot{q} = \dot{q}_{int} = 0$, (Fig. 2). Thus the temperature boundary conditions read as

$$T_B = T_h = T_0 + \Delta T = 1373K \texttt{ for } z = 0 \texttt{ (on the ampoule lower wall)} \quad (1)$$

$$T_B = T_h = T_0 + \Delta T = 1373K \texttt{ for } r = d/2 \texttt{ (on the crucible lateral wall)} \quad (2)$$

$$\dot{q}_{int} = 0 \texttt{ for } z = h \texttt{ (on the free surface)} \quad (3)$$

$$T_A = T_c = T_0 = T_{ref} = T_{\texttt{mean melt}} \ \texttt{(reference temperature)} \tag{4}$$

where T_0 is the reference temperature which can be taken equivalent to that of the cold wall (T_A) or the mean of the hot and cold wall temperatures ($(T_A + T_B)/2$). Since in the present model, the geometry is cylindrical thus T_0 is chosen as the *mean* temperature of the melt. Moreover, since the melt is under isothermal conditions thus the choice of the value of T_0 should satisfy the Boussinesq approximation (for which $\Delta T = T_B - T_0 < 30$).

In the system of cylindrical coordinates, $\mathbf{x} = (r, \phi, z)^T$, the governing equations for the physical problem (of combined natural/thermocapillaire convection) shown in Fig. 1 are

$$\nabla \cdot \mathbf{u} = 0 \tag{5}$$

$$\frac{\partial \mathbf{u}}{\partial t} + \mathbf{u} \cdot \nabla \mathbf{u} = -\frac{1}{\rho} \nabla p + \nu \nabla^2 \mathbf{u} + g\beta_T (T - T_0) \tag{6}$$

$$\frac{\partial T}{\partial t} + \mathbf{u} \cdot \nabla T = \alpha \nabla^2 T \tag{7}$$

where ρ, $\nu = \mu/\rho$, g ,β_T and $\alpha = k/\rho cp$ are the density, kinematic viscosity, gravity, thermal expansion coefficient and the thermal diffusivity of the melt, respectively (with cp is the specific heat melt). Furthermore, $\mathbf{u} = (u_r, u_\phi, u_z)^T$, p and T are the velocity, pressure and temperature fields, written in the system of cylindrical coordinates, (r, ϕ, z), respectively.

In the derivation of the above so-called Boussinesq-Oberbeck equations, the Boussinesq approximation is adopted, the flow regime is assumed to be laminar and the melt is considered as incompressible. Also, neither heat generation (Joule heating) nor absorption are considered, furthermore, no heat transfer by radiation is assumed. The thermophysical properties of the germanium melt are assumed constant and compiled from [13, 14]. These properties are given in Table 1[1]. In addition to the density dependence of temperature, $\rho(T)$, which is evidently included in the Boussinesq approximation, the surface tension dependence of temperature, $\sigma(T)$, is also taken into account in the present model. For the assumption of small temperature variations, the surface tension may be expressed in terms of $T - T_0$ as:

$$\sigma(T) \approx \sigma_0(T_0) - \gamma(T - T_0) \tag{8}$$

where $\sigma_0(T_0)$ is the mean surface tension of melt at the reference state 0 (as mentioned earlier) and γ represents the *coefficient of temperature*: $\gamma = \partial\sigma/\partial T$.

2.2. **Velocity and temperature boundary conditions.**

2.2.1. *Velocity boundary conditions.* On the rigid crucible/ampoule walls: The Ge melt under consideration is bounded from below and tangentially (from the side) by the rigid and stationary walls of the crucible/ampoule system. Thus

$$\mathbf{u} = 0 \tag{9}$$

On the free surface (interface melt/vacuum): Along the free surface separating the two immiscible fluids, melt (1) and vacuum gas (2), (see Fig. 2), the forces acting on the surface adjacent elements, of the fluids (1) and (2) should be balanced. This leads to the equilibrium:

Forces acting on the surface elements of fluid (1) = Forces acting on the surface elements of fluid (2)

[1]Note that the temperature coefficient value is estimated to be 0.104×10^{-4} N/m K.

If the shape (surface) of the free surface is assumed to be *planer* (plane interface) the surface tension is constant and the above equilibrium reads as

$$\left\{-p\mathbf{I}+\mu\left[\nabla\mathbf{u}+(\nabla\mathbf{u})^T\right]\right\}_{(1)}\cdot\mathbf{n}=\left\{-p\mathbf{I}+\mu\left[\nabla\mathbf{u}+(\nabla\mathbf{u})^T\right]\right\}_{(2)}\cdot\mathbf{n} \tag{10}$$

where $-p\mathbf{I}+\mu\left[\nabla\mathbf{u}+(\nabla\mathbf{u})^T\right]$ is the stresses tensor, expressed in terms of the pressure, p, and the viscous stress, $\mu\left[\nabla\mathbf{u}+(\nabla\mathbf{u})^T\right]$, by the surface unit. In the above equation μ represents the dynamic viscosity, $\mathbf{I}$ is the identity tensor and $\mathbf{n}$ is the normal vector unit oriented out of the melt (Ge) (1) into the ambient gas vacuum (2) (see Fig. 2).

In the case of a *curved* interface, however, the surface tension *varies* along the interface (located on the plane $z=\xi(r,\phi)$) and generally the following equilibrium may be adopted

$$\left\{-p\mathbf{I}+\mu\left[\nabla\mathbf{u}+(\nabla\mathbf{u})^T\right]\right\}_{(1)}\cdot\mathbf{n}+\{\sigma(\nabla\cdot\mathbf{n})\mathbf{n}-\mathbf{t}\cdot\nabla\sigma\}_{(1)}=\left\{-p\mathbf{I}+\mu\left[\nabla\mathbf{u}+(\nabla\mathbf{u})^T\right]\right\}_{(2)}\cdot\mathbf{n} \tag{11}$$

where the first additional term $\sigma(\nabla\cdot\mathbf{n})$ is the *Laplace* pressure, in which $\nabla\cdot\mathbf{n}$ represents the *mean* curvature of the interface and the second additional term is the scalar product of $\nabla\sigma$ and the tangential vector unit $\mathbf{t}$ (which is the orthogonal projection of a vector on radial plane defined by $\mathbf{n}$, see Fig. 2).

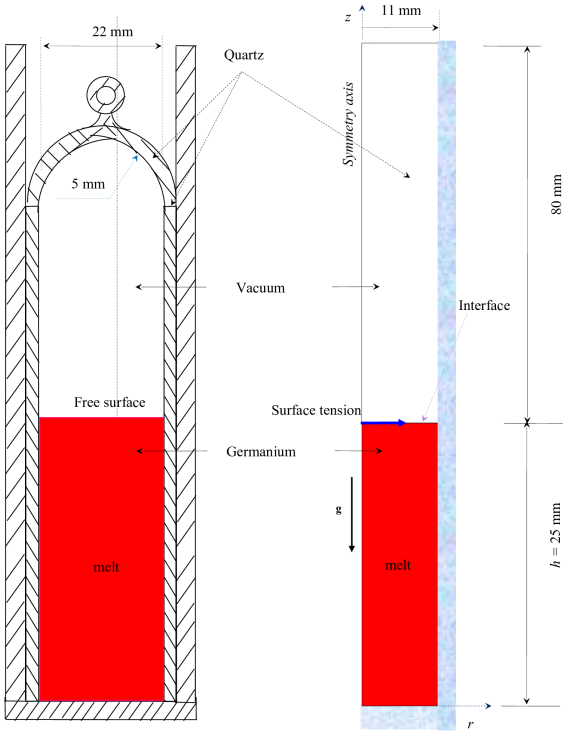

FIGURE 1. Schematic of the experimental setup (left), the simulated axisymmetric (2D) domain (right).

2.2.2. *Temperature boundary conditions.* On the melt free surface, the temperature should be *continuous*. In the case where the *ambient* temperature distribution, T_{amb}, in the region near the interface, is not unknown, the Newton law is used. In the presence of

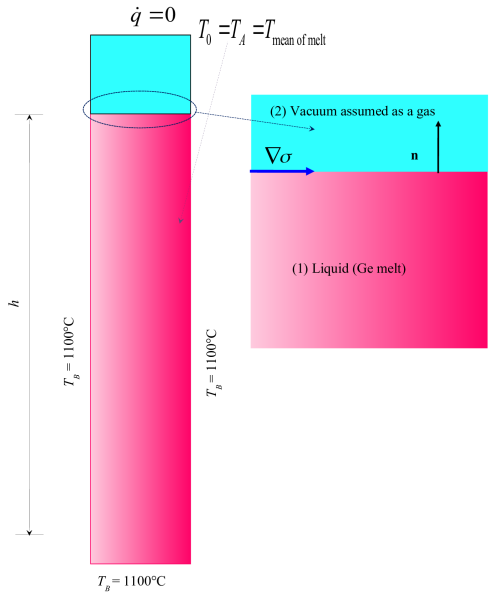

FIGURE 2. Typical representation of boundary and interface conditions: the thermal boundary conditions imposed on the system (left) and the free surface separating two immiscible fluids: the Ge melt (1) and the vacuum which assumed as a gas (2) (right).

an interface, separating two immiscible fluids, and in the case where the radiation heat transfer is neglected, the Newton law reads as

$$k\mathbf{n}\cdot\nabla T = -h_{conv}(T - T_{amb}) = -h_{conv}(T_{int} - T_{amb}) \quad \texttt{(across the interface)} \tag{12}$$

where h_{conv} is the convection heat transfer coefficient. The equation (9) describes the heat flux by conduction "$k\mathbf{n}\cdot\nabla T$", through the interface, to the heat flux by convection "$h_{conv}(T_{int} - T_{amb})$", expressed in terms of the temperature of the interface surface "T_{int}" and the ambient temperature, T_{amb}, given at a certain distance, $\mathbf{x}$, from the interface. Here $T_{amb}\mathbf{x}$ represents, thus, the temperature at the reference state ambient denoted by "amb" (that of the external medium "i.e. the gas (vacuum) (2)"). Following the value of h_{conv} two limits can be presented: The first is the limit when $h_{conv} \to \infty$, the external temperature T_{amb} should be imposed on the melt free surface,

$$T \equiv T_{int} = T_{amb} \quad \texttt{(Dirichlet condition)} \tag{13}$$

this is a good approximation if the thermal diffusivity of the external medium "gas" is much higher than the melt, [9]. The present problem is not concerned by such an interface boundary condition since it was assumed that the vacuum is a gas with neglected thermal diffusivity. The second limit is when $h_{conv} \to 0$ thus:

$$k\mathbf{n}\cdot\nabla T = 0 \quad \texttt{(Neumann condition)} \tag{14}$$

TABLE 1. Thermophysical properties of the Germanium melt [13, 14].

Property	Value
Thermal conductivity, $k[W/Ccm]$	0.39
Density, $\rho[g/cm^3]$	5.5
Specific heat, $cp[J/Cg]$	0.39
Kinematic viscosity, $\nu[cm^2/s]$	0.0013
Thermal expansion coefficient, $\beta_T[C^{-1}]$	1×10^{-4}

The equation (14), adopted for the experimental crucible setup shown in Fig.1, describes an interface adiabatic and thus justifies the boundary condition used in the experimental work that the flux on the interface is set to be zero (as mentioned earlier).

2.3. **Dimensionless equations.** For the physical problem shown in Fig.1, the following characteristic scales are adopted: d for the length[2], d^2/ν for the time, $\gamma\Delta T d^2/\rho\nu$ for the velocity, $\gamma\Delta T d^2/d$ for the pressure and ΔT for the temperature. Thus, both the independent dimensionless variables ($\mathtt{R}, \Phi, Z$ and τ) and the dependent dimensionless variables (U_r, U_ϕ, U_z, P and Θ) are given as $R = r/d, \Phi = \phi/d, Z = z/d, \tau = t/(d^2/\nu)$, $U_r = u_r/(\gamma\Delta T d^2/\rho\nu), U_\phi = u_\phi/(\gamma\Delta T d^2/\rho\nu), U_z = u_z/(\gamma\Delta T d^2/\rho\nu)$, $P = p/(\gamma\Delta T/d)$ and $\Theta = (T - T_0)/\Delta T$, where $U = (U_r, U_\phi, U_z)^T$, P, and Θ are the dimensionless velocity, pressure and temperature fields, respectively. Thus, the above governing equations in dimensionless forms read as

$$\nabla \cdot \mathbf{U} = 0 \tag{15}$$

$$\frac{\partial \mathbf{U}}{\partial \tau} + Re\, \mathbf{U} \cdot \nabla \mathbf{U} = -\nabla P + \nabla^2 \mathbf{U} + (Gr/Re)\, \Theta \mathbf{e}_z \tag{16}$$

$$\frac{\partial \Theta}{\partial \tau} + \mathbf{U} \cdot \nabla \Theta = (1/Pr)\, \nabla^2 \Theta \tag{17}$$

where the dimensionless numbers $Re = \gamma\Delta T d/\rho\nu^2$, $Gr = g\beta_T \Delta T d^3/\nu^2$, $Pr = \nu/\alpha = 0.0075$ and $Bd = Gr/Re$ characterizing the combined natural/Marangoni convection in the cylindrical (3D) geometry, shown in Fig.1, are given in Table 2. Furthermore, the present configuration geometry (3D) is characterized by the aspect ratio: $\Gamma_{3D} = h/d = 25/22 = 1.14 \approx 1$.

TABLE 2. The dimensionless numbers characterizing the problem of combined natural/Marangoni convection flows.

Re	Gr	$Bd = Gr/Re$	Ra	Ma
$2.46 \times 10^3 \Delta T$	$7.4 \times 10^5 \Delta T$	300	$5.55 \times 10^3 \Delta T$	$18.45 \Delta T$

2.4. **Dimensionless velocity and temperature boundary conditions.** By referring to the figure 2 and the above characteristic scales, the dimensionless boundary conditions associated with the present model are as follows.

[2]Generally, the height of the melt is taken as the characteristic length for the problem of pure natural convection. In the present problem (combined convection), however, the interface length (diameter) is taken as the characteristic length.

2.4.1. *On the rigid crucible/ampoule walls.* The velocity and temperature boundary conditions on the rigid and isotherms crucible/ampoule walls, located at $Z = 0$ (on the ampoule lower wall) and $R = R/d = 1/2$ (on the crucible radial wall), respectively, read as

$$\mathbf{U} = 0, \Theta = 0 \ \texttt{for} Z = 0 \ \texttt{and} R = 1/2 \tag{18}$$

Velocity boundary conditions. If the shape of the interface, located on the axial plane given by $Z = \Xi(R, \Phi)$, is assumed to be curved, the stress balance on the interface may be obtained by the non-dimensionalization and simple projection of the equation (11) on the (R, Φ, Z) directions. Moreover, in the case of the presence of buoyancy "$Gr \neq 0$" (as in the present case), the surface *deformations*, created by the flow, should been taken into account, and *corrections* to the Boussinesq-Oberbeck equations should be included in order to ensure the *consistence*. Thus, it should be assumed *only* that the free surface is stationary, [9]. Therefore, the stresses balance on the interface reads as

$$\mathbf{t} \cdot [\nabla \mathbf{U} + (\nabla \mathbf{U})^T]\mathbf{n} + (\mathbf{t} \cdot \nabla)\Theta = 0 \tag{19}$$

where $\mathbf{t}$ and $\mathbf{n}$ represent the dimensionless tangential and normal vector units, respectively.

Temperature boundary conditions. In dimensionless form, the thermal boundary condition, given by (12), reads as

$$\mathbf{n} \cdot \nabla\Theta = -Bi[\Theta - \Theta_{amb}] \ \texttt{(on the the free surface} \ \Theta - \Theta_{int}) \tag{20}$$

where $Bi = h_{conv}d/k$ is the Biot number. As mentioned early, instead the equation (12), the present model is concerned by the equation (14) which, in dimensionless form, reads as

$$\mathbf{n} \cdot \nabla\Theta = 0 \ \texttt{(on the the free surface)} \tag{21}$$

thus for the present configuration: $Bi = 0$.

2.4.2. *Boundary conditions at the axis of symmetry (applied only for 2D model).* The symmetry boundary conditions are used at the axis of symmetry. For physical finite results, it is required that the radial velocity component be zero. Thus

$$U = 0, \partial V/\partial R = 0, \mathbf{n} \cdot \nabla\Theta = 0 \ \texttt{for} \ R = 0 \tag{22}$$

3. Numerical resolution

To express convection in a 2D (axisymmetric) configuration as shown in Fig. 1, the equations for mass conservation (15), momentum (16) and energy balances (17), with associated boundary conditions, equations (18), (19), (21) and (22), for the combined natural/Marangoni convection melt flows in the crucible must be written in the 2D (axisymmetric) system of coordinates and solved numerically. Results are obtained by using the COMSOL multiphysics CFD package [15]. Further details about the solution methodology are given in the references [16, 17].

4. Results and discussion

Firstly, the non-dimensional numbers characterizing the combined convection melt flows are predicted and given in Table 2. Values are predicted for various values of ΔT. Recall that $\Delta T = T_B - T_0$ should be chosen lesser than 30.

4.1. **Axisymmetric pure thermocapillary convection in the Ge melt.** The qualitative vortex structures, i.e. the main toroidal vortex and the weak secondary vortex in the melt, for the present crucible configuration, exist at all Reynolds numbers. Since the Prandtl number of germanium melt is Pr = 0.0075 (see Table 2), accordingly to the so-called *conductive inertial limit*, [9], it is expected that Marangoni (thermocapillary) convection effects are insignificant in the range of $Re \ll Pr^{-1/3} \approx 1540$, but they should become significant for $Re \gg Pr^{-1/3}$. In order to verify these trends, numerical simulations were carried out for the Re numbers in the range between 1 and 2.12×10^4 (which corresponds to ΔT between ~ 0 and 8.6 , see Table 2).

For small Reynolds numbers, numerical simulations show that the strength of the flow is constant (as expected). Example on the time-dependent flow structures and temperature distributions for Re = 1000 (i.e. $\Delta T \approx 0.4$) is shown in Fig. 3. For this quite small Reynolds number, the flow is composed of the main toroidal vortex that rotates clockwise or counterclockwise[3] and the weak secondary vortex, which is developed near the lower right corner of the crucible. The maximum dimensionless velocity reached in the melt, after about 1 hour (i.e. $\tau = 1$)[4] , is 1.563×10^{-5} (value reached on the free surface). By comparing the two velocities reached after 1 hour for the two cases of the Reynolds numbers (1000 and for instance for 246)[5] , one can easily verify that the scaled amplitude of velocity (i.e. $\|\mathbf{U}\| = \|\mathbf{u}/u_c\|$) is almost constant and relatively independent of the Reynolds number. For Re=1000, the velocity and temperature distributions, on the free surface, and the local Nusselt numbers on the surface between the melt and solid (crucible side wall), at different times, are also shown in Fig. 3. The predicted local Nusselt number shows *fluctuations* which clearly indicate the *oscillatory* nature of thermocapillary flows in the melt.

When the value of the Re number is increased the inertial effects become significant and it is expected that the scaled amplitude of velocity will decay as $Re^{-1/3}$ and finally become independent of Re, [9]. In this case the streamlines become increasingly non-symmetric and the center of the main vortex is shifted towards the warm regions of the melt (i.e. close to the upper right corner of the melt). Example on the time-dependent flow structures and temperature distributions for Re=3400 (which corresponds to $\Delta T \approx 1.38$) is shown in Fig. 4. Examination of the forms of streamlines, shown in Fig. 3 and 4, shows clearly the previous trends. For Re=3400, the maximum dimensionless velocity reached in the melt, for instance after about 1 hour, is 1.537×10^{-5} . By comparing the two velocities reached after 1 hour for the cases of Re=1000 and 3400, one can easily verify that the Marangoni convective effects are insignificant than expected (compare Fig. 3 and 4).

When the Reynolds number is increased further (for instance to $\mathrm{Re} = 2.28 \times 10^4$ (i.e. $\Delta T \approx 5.2$), the vortex creates a nearly *inviscid core*, [9], in which the vorticity Ω varies linearly with the axial direction Z and which is bounded by viscous boundary layers. The maximum velocity on free surface after 1 hour is 1.296×10^{-5}. By comparing the two velocities reached after 1 hour for the both cases Re=3400 and $\mathrm{Re} = 2.28 \times 10^4$, one can easily verify that the scaled amplitude of velocity is very close and thus the velocity becomes slightly independent of Re as expected. It should be emphasized here that the flow presents signs of *instability* at the early times when the value of the Re is further increased and approached the value of $\approx 2.12 \times 10^4$ (i.e. $\Delta T \approx 8.6$).

[3]In fact, the sense of rotation changes with time.

[4]In fact, $t = (d^2/\nu)\tau \approx 3720\tau$, thus the non-dimensional time $\tau = 1$ corresponds approximately to 1 hour.

[5]For Re= 246, the velocity reached on free surface after 1 hour is 1.563×10^{-5}.

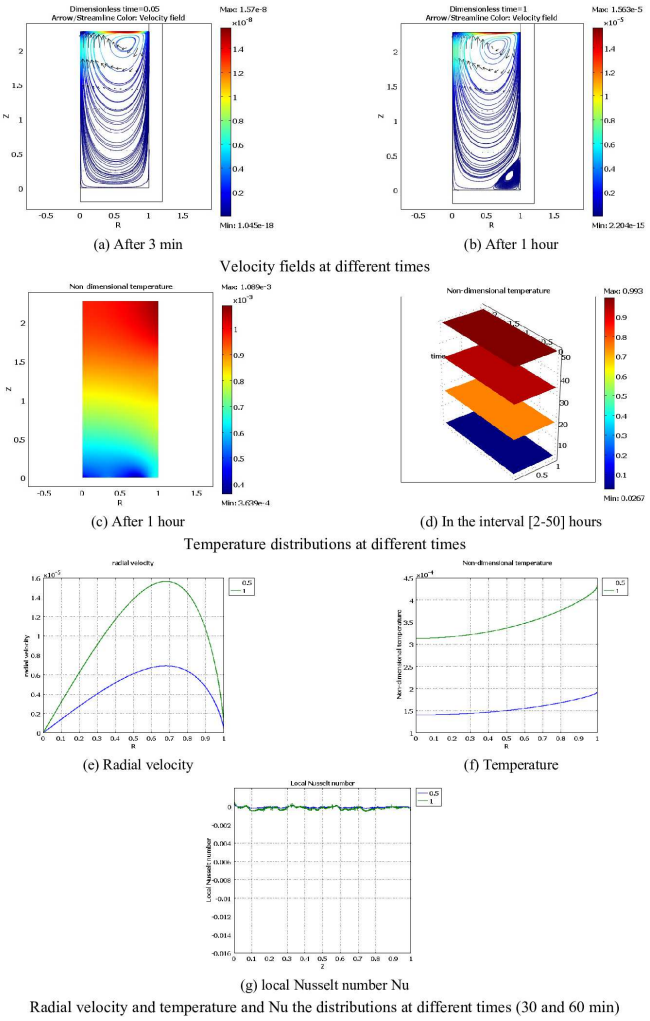

FIGURE 3. Time-dependent flow and temperature fields in the germanium melt (Pr=0.0075) for Re=1000, (with Gr=0 and Bi=0).

4.2. **Axisymmetric pure natural convection flow in the Ge melt.** The other important driving force for an axisymmetric convection flow in the germanium melt is buoyancy. It is well known that when the heating is from below, as in the present crucible system, the melt flow is similar to the Rayleigh-Benard convection problem and the conductive state (u = 0) can be *unstable* [9]. In addition to the heating from below, the present configuration is also heated from the side. Thus, it will be subjected to very complex convective motions. In order to give further insight into the nature of melt flows, in the crucible, numerical simulations were carried out for the pure natural convection flow for the Gr numbers in the range between 150 and 2.73×10^6 (i.e. ΔT between ~ 0 and 3.7).

The qualitative vortex structures (both the primary and the secondary convection cells in the melt) exist at all tested Grashof numbers. For small Grashof numbers, Fig. 5 shows the predicted streamlines and isotherms in the melt for Gr=1000 (i.e. Ra=7.5) at different times. The flow structure is composed from the main counterclockwise rotating vortex (primary convection cell), formed at early times (Fig. 5a), which persists in the

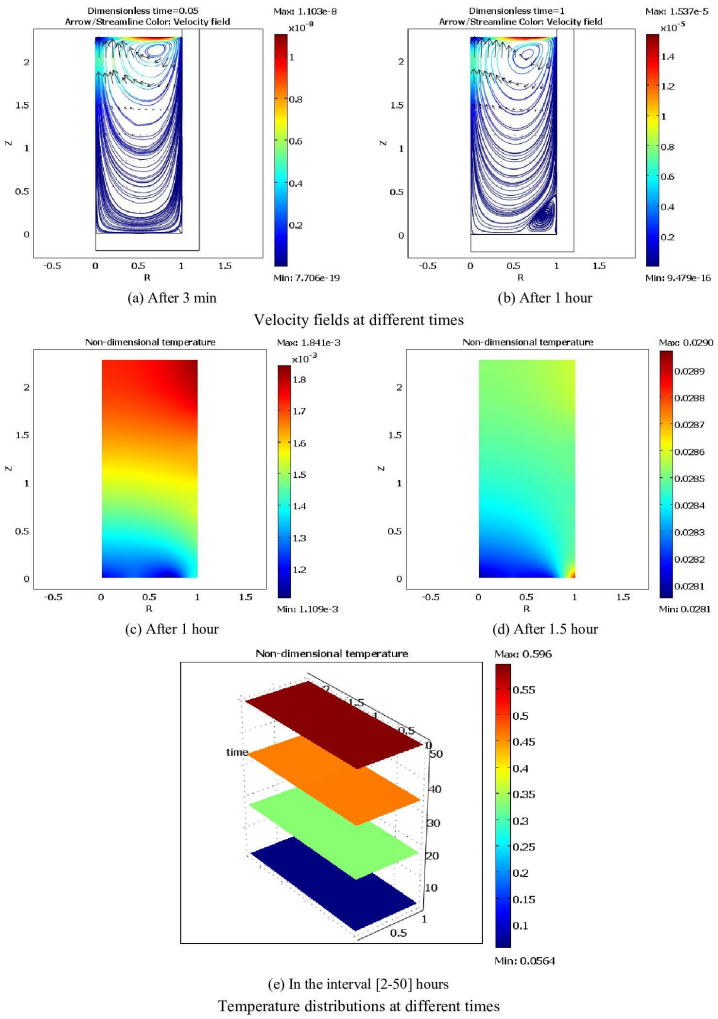

FIGURE 4. Time-dependent flow and temperature fields in the germanium melt (Pr=0.0075) for Re=3400, (with Gr=0 and Bi=0).

melt and expands with time until reaching the entire domain. At the time $\tau \approx 1.5$ another clockwise rotating vortex appears in the melt (near the upper right corner). This vortex (secondary convection cell) will grow in size with time until occupy the upper half region of the domain (see Fig. 5).

When the Gr is further increased, for instance to $\mathrm{Gr} = 1.5 \times 10^5$, the previous predicted trends are observed. Moreover, it should be emphasize that the strength of flow is increased when Gr value is increased as expected. The only difference, between these two Grashof cases, subsists in the time of appearance of secondary convection cell. Indeed, the time of appearance will decay when Gr reaches values higher than ≈ 3000. Numerical simulations also showed that the value of $\mathrm{Gr} \approx 1.63 \times 10^5$, (i.e. $\mathrm{Ra} \approx 1222.5$) represents a critical value for flow transition. Indeed, when the Gr number is further increased up to the above Gr value, the predicted flow structures are considerably altered. An example on the time-dependent flow structures and temperature distributions for $\mathrm{Gr} = 1.02 \times 10^5$ (which corresponds to $\Delta T \approx 1.38$) is shown in Fig. 6. Moreover, numerical simulations showed

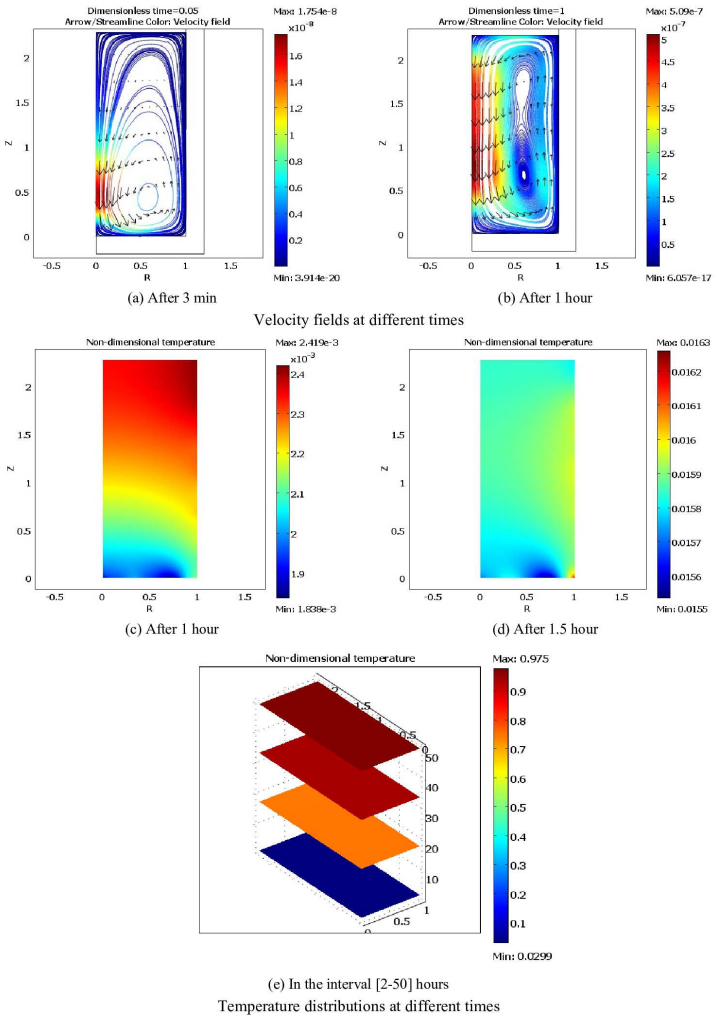

FIGURE 5. Time-dependent flow and temperature fields in the germanium melt (Pr=0.0075) for Gr=3400 (i.e. Ra=7.5), (with Re=0).

that the value $\mathrm{Gr} \approx 2.73 \times 10^6$ (i.e. $\Delta T \approx 3.7$), represents another critical value for flow structure transition[6].

4.3. **Axisymmetric combined natural/thermocapillary convection flows in the Ge melt.** For small Grashof and Reynolds numbers, numerical simulations showed that the flow is axisymmetric as expected. An example on the flow structures and temperature distributions (for Re=1000 and Gr=1000 i.e. Bd = 1) is shown in Fig. 7. Since thermocapillary convection is commonly accompanied by axial temperature gradients; thus the Marangoni flow is altered by the effect of buoyancy forces (see and compare the flow fields shown in Fig. 3, 5 and 7). The flow is mainly driven by buoyancy during early times (Fig. 7a). Since the Re number is small, the Marangoni flow, formed in the upper region of melt, is characterized by a vortex of nearly equal strength of circulation but with different sense (direction) of rotation (Fig. 7b). Depending on the sense of rotation the

[6]It should be emphasize that the present paper is not concerned by the flow transition and stability.

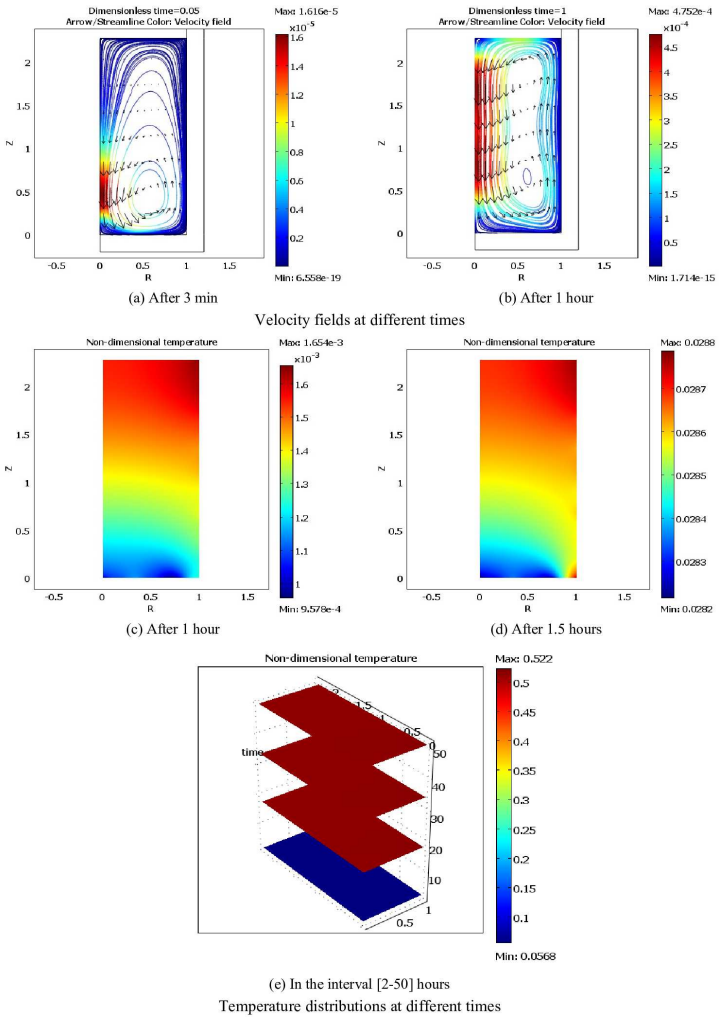

FIGURE 6. Time-dependent flow and temperature fields in the germanium melt (Pr=0.0075) for Gr=1.02×10^6 (i.e. Ra=7650), (with Re=0).

weak thermocapillary surface forces, acting often in the radial positive direction, either suppress (Fig. 7b) or improve the main vortex motion (Fig. 7c).

The relative strength of thermocapillary forces compared to buoyancy forces depends on the dynamical Bond number, $Bd = Gr/Re = \rho g \beta_T d^2/\gamma$. Hence, natural convection maybe ignored when $Bd \to 0$ (i.e. the length scale tends to zero $L_c = d \to 0$). In the present crucible configuration, however, Bd$\sim$300, it is expected that the Marangoni are small and heat transfer is mainly dominated by natural convection. An example on the flow structures and temperature distributions for Re=3400 and Gr = 1.02×10^5 (see Table 2) is shown in Fig. 8. The figure shows clearly the above trend. Indeed, by comparing the streamlines forms in Fig. 8 and 4, one can easily identify that the Marangoni flow is weakened by natural convection.

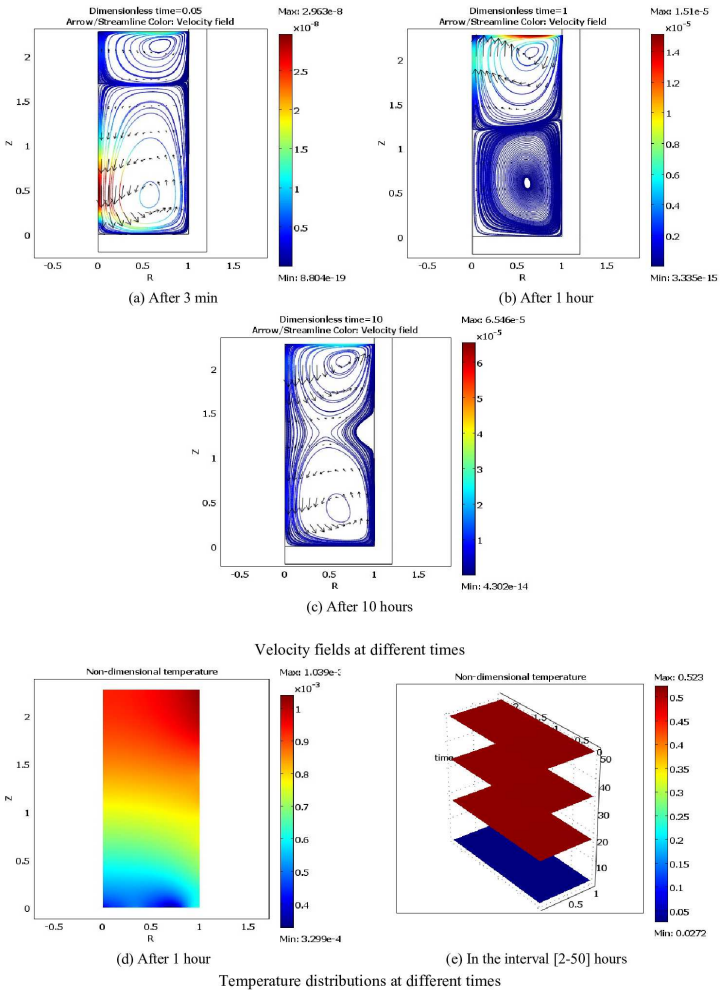

FIGURE 7. Streamlines and isotherms in the Ge melt (Pr=0.0075) for Re=1000 and Gr=1000 (i.e. Bd=1), (with Bi=0).

5. Conclusion

A mathematical model to describe the combined natural/thermocapillary convection fluid flows is presented. The model is adapted to that of the combined natural/ thermocapillary axisymmetric convection flows developed in the germanium melt. The melt in the experimental crucible setup was assumed to be under isothermal conditions.

The most important properties of the *nonlinear* convective flows in the germanium melt are examined by using a simplified version of the model (axisymmetric). Numerical simulations are carried out to predict the axisymmetric thermocapillary, natural and combined natural/thermocapillary convective flows in the melt. The predicted properties of the axisymmetric thermocapillary, natural and combined natural/thermocapillary convective flows in the germanium melt slightly agree with the experimental results of the study of dissolution of silicon into a germanium melt [11, 12]. Indeed, as in experiments, numerical simulations showed that the nature of convective flows develop in the melt exhibit flow

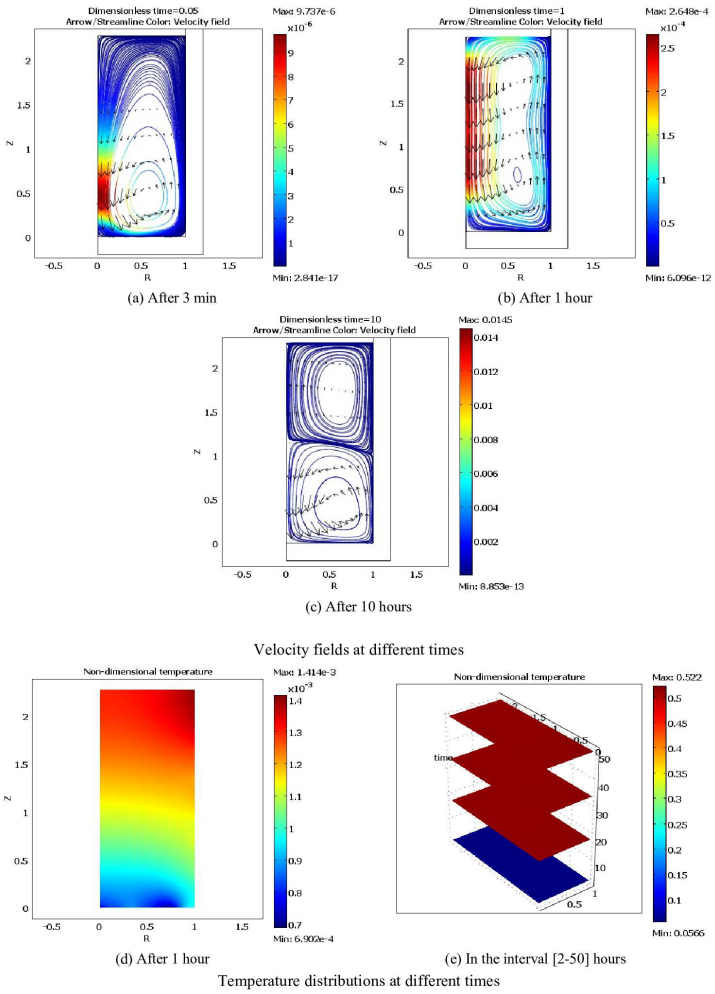

FIGURE 8. Streamlines and isotherms in the Ge melt (Pr=0.0075) for Re=3400 and Gr=1.02×10^6 (i.e. Bd=300), (with Bi=0).

instabilities and transitions. In particular, it was shown that the Marangoni convection has an important effect. Flow instability leads to melt inhomogeneity and thus can play an important role on the dissolution behavior. These trends can strongly affects the *mixing* in the melt and the *shape* of the dissolution interface as reported in [12].

Possible deviations from the experimental results of the present axisymmetric model predictions are essentially due to non-cylindrical surface deformations, contamination of the free surface, temperature dependent material parameters, and momentum and heat transfer to the ambient gas. These effects are neglected in the present model.

Acknowledgement: Support from NSERC (Natural Sciences and Engineering Research Council of Canada) is gratefully acknowledged.

References

[1] Kasper, E., Paul, D.J., (2005), Springer-Verlag Berlin.
[2] Dost, S., Lent, B. (2007), Elsevier, Amsterdam, the Netherlands.
[3] Armour, N., Yildiz, M., Yildiz, E., Dost, S. (2008), ECS Transactions, 16, pp. 135146.
[4] Prasad, V., Zhang, H., Anselmo A.P. (1997), In Advances in heat transfer, Acad. Press, 30, pp. 313-435.
[5] Bohm, J., Ludge, A., Schroder, W., (1994), Chap. 4. In: Handbook of Crystal Growth, Vol. 2A, D.T.J. Hurle (ed.), Elsevier, North-Holland.
[6] Van der Eerden J.P., (1993), Chap. 6. In Handbook of Crystal Growth, Vol. 1A, ed. By Hurle, D.T.J., Elsevier, North-Holland.
[7] Bliss, D.F. (2010), Chapter 7. Part B, p. 207, in Springer Handbook of Crystal Growth, G. Dhanaraj, K. Byrappa, V. Prasad, M. Dudley (Eds.), Springer-Verlag Berlin.
[8] Nishijima, Y., Nakajima, K., Otsubo, K., Ishikawa, H., (2000), J. Cryst. Growth, 208, pp. 171178.
[9] Kuhlmann, H.C., (1999), Springer-Verlag Berlin Heidelberg.
[10] Kakimoto K., (2004), Crystal Growth - from Fundamentals to Technology. Muller, G.; Metois J.-J. and Rudolph P. (Editors), Elsevier, Amsterdam.
[11] Armour, N., Dost, S. (2009), J. Cryst. Growth, 311, pp. 780782.
[12] Armour, N., Dost, S., Lent, B., (2007), J. Cryst. Growth, 299, pp. 227233.
[13] Sampath, R., Zabaras, N., (2001), J. Comp. Physics, 168, pp. 384411.
[14] Yildiz, M., (2005), PhD thesis, University of Victoria, Canada.
[15] COMSOL Multiphysics Modeling Guide (2008).
[16] Mechighel, F., Armour, N., Dost, S., Kadja, M., (2014), CMES: Computer Modeling in Engineering and Sciences, 97(1), pp.5380.
[17] Mechighel, F., Armour, N., Dost, S., Kadja, M., (2011), TWMS J. App. Eng. Math., 1(2), pp. 200-222.

Dr. Farid Mechighel is a teacher and researcher at the mechanical engineering department, university of Annaba. His main research is in the area of computational modeling of crystal growth, with particular application to innovative techniques, such as Liquid Phase Diffusion, Bridgman, etc. Moreover, he is interested in domains such: solidification phenomena.

Dr. Neil Armour is a Researcher in the Crystal Growth Laboratory at the University of Victoria. Neil received his Ph.D. from the University of Victoria in 2012. His undergraduate education is in physics and astrophysics from the University of California, Berkeley. His current research is in the experimental study of crystal growth. Particularly, his research focuses on compound semiconductor production and the underlying mass transport processes

Dr. Sadik Dost is Professor and Director of the Crystal Growth Laboratory at the University of Victoria. He has obtained his Ph.D. in Istanbul Technical University in 1974. His current research combines experimental and theoretical study of crystal growth of semiconducting bulk single crystals from the liquid phase with particular focus on materials like Cadmium Zinc Telluride (CZT) and Silicon Germanium (SiGe) that are needed for a variety of applications mainly for solar energy conversion, medical imaging, and infra-red and security devices.